Holm, Andreas; Wünderlich, Dirk; Groth, Mathias; Börner, Petra

Impact of vibrationally resolved H_2 on particle balance in Eirene simulations

Published in:
Contributions to Plasma Physics

DOI:
10.1002/ctpp.202100189

Published: 01/06/2022

Document Version
Publisher's PDF, also known as Version of record

Received: 1 October 2021 | Revised: 16 December 2021 | Accepted: 5 January 2022 | Published on: 7 February 2022

DOI: 10.1002/ctpp.202100189

ORIGINAL ARTICLE

Contributions to Plasma Physics

Impact of vibrationally resolved H_2 on particle balance in Eirene simulations

Andreas Holm[1] | **Dirk Wünderlich**[2] | **Mathias Groth**[1] | **Petra Börner**[3]

[1]Department of Applied Physics, Aalto University, Aalto, Finland

[2]Max-Planck-Institut für Plasmaphysik, Garching, Germany

[3]Institut für Energie- und Klimaforschung – Plasmaphysik, Forschungszentrum Jülich GmbH, Jülich, Germany

Correspondence
Andreas Holm, Aalto University, P.O. Box 11000, FI-00076 Aalto, Finland.
Email: andreas.holm@aalto.fi

Funding information
Academy of Finland, Grant/Award Number: 13330050; EUROfusion, Grant/Award Number: 633053

Abstract

To evaluate the impact of transport of metastable, vibrationally excited states of the hydrogen molecule in dense and cold plasmas each vibrational state must be simulated as an individual species. Eirene neutral gas simulations of a one-dimensional flux-tube using a metastable-resolved model indicate a 30–50% decrease in the effective dissociation rate compared to simulations using a metastable-unresolved setup, which consider a single molecular species. Zero-dimensional Eirene simulations omitting transport effects predict a 25–65% decrease in the effective dissociation rate due to differences between the metastable-unresolved AMJUEL and the metastable-resolved H2VIBR rates available in Eirene. The exclusion of molecular hydrogen depletion via electronically excited states and vibrational transitions $v \rightarrow v \pm N, N > 1$ from the metastable-resolved rates reduce the effective dissociation rate. By accounting for the difference caused by the different collisional-radiative treatment of the metastable-resolved rates compared to the metastable-unresolved rates, transport effects are expected to be relevant under detached divertor conditions. It is, however, not possible to individually assess the role of the collisional-radiative processes and transport on the effective dissociation rate using the currently available atomic and molecular rates for the metastable-resolved and metastable-unresolved Eirene setups.

KEYWORDS

collisional-radiative model, Eirene, hydrogen molecules, vibrational states

1 | INTRODUCTION

Numerical fusion boundary plasma simulations rely on kinetic neutral particle codes to evaluate neutral gas transport and plasma sinks and sources resulting from neutral processes. The Eirene code[1] is a well-established kinetic neutral code used in scrape-off layer (SOL) plasma code packages such as SOLPS-ITER,[2,3] EMC3-EIRENE,[4] and EDGE2D-EIRENE.[5,6] Eirene evaluates the transport and reactions of the neutral species using atomic and molecular (A&M) data by applying Monte Carlo methods, calculating macroscopic plasma parameters such as particle, momentum, and energy sinks and sources and the resulting densities for the neutrals.[1] The role of molecular effects is expected to be especially important in carbon devices, as a majority of the target fluxes are recycled as molecules[7] but the role of molecules may be smaller in metallic devices.[8] However, due to high target fluxes and divertor densities predicted

in metallic next-step devices, such as ITER, the role of plasma-neutral friction, and molecular-assisted production of excited atoms may be significant.

This work evaluates the impact of simulating transport of vibrational states in Eirene for pure hydrogen plasmas on the molecular (H_2) sinks and transport in simplified zero- and one-dimensional geometries. Eirene commonly simulates H, H_2, H^-, and H_2^+ as single species and does not explicitly evaluate transport of the 15 vibrational states of electronic ground-state H_2. This "metastable-unresolved" setup (e.g., ADAS[9] terminology), does not individually evaluate the transport of vibrational states, which may result in non-local effects impacting the quasi-steady-state vibrational distribution of the molecules. Many H_2 reaction rates increase strongly with increasing vibrational level of the ground state molecule: thus, deviations of the local H_2 vibrational distribution from a quasi-steady-state collisional-radiative (CR) equilibrium vibrational distribution ($P_{eq}(v)$) impacts the effective molecular sinks and sources. Consequently, deviations from the $P_{eq}(v)$ will affect both the production of H_2^+ and H^-, which are the reactants in molecular-assisted processes, and spectroscopic analysis that use the vibrational temperature, that is derived assuming a $P_{eq}(v)$.[10]

One of the first metastable-resolved Eirene setups, which considers transport for each of the H_2 vibrational states, predicted an attached plasma solution, whereas a metastable-unresolved setup predicted a detached plasma solution for the same upstream density.[11] Previous work has shown that transport of vibrationally excited states should be considered[12] and such non-local effects were assumed to cause this re-attachment of the plasma solution when changing from the metastable-unresolved to the metastable-resolved simulations. This work shows that non-local effects are partly responsible for the observed behaviour, but that scarcity of the underlying A&M data available for the metastable-resolved Eirene setup also contribute to the re-attachment observed in ref. [11]. In addition, this work highlights that the role of the two effects cannot presently be individually evaluated using Eirene due to code legacy. Finally, an overview and assessment of the currently available A&M data for the metastable-resolved and metastable-unresolved Eirene setups are presented, potential shortcomings of these two frequently used Eirene setups are identified, and future improvements are recommended.

2 | MOLECULAR MODEL SETUP

2.1 | The Eirene model

This work evaluates two molecular setups in the kinetic neutral code Eirene: one metastable-resolved and one metastable-unresolved. The metastable-unresolved Eirene setup simulates the transport and reaction chains of a single H_2 species, assuming the metastable states to be at local vibrational quasi-steady-state equilibrium $P_{eq}(v)$ with the molecular ground state. The metastable-resolved Eirene setup individually considers transport and reaction chains for each of the 15 vibrational H_2 species. Both setups consider the same molecular reaction chains into H atoms and H^+ ions via the charged test species H_2^+ and H^-. The setups use a quasi-steady-state approximation for the charged test species and include the same reactions involving H_2^+ and H^-. Thus, molecular-assisted recombination, dissociation, and ionization are considered by both setups and any differences in the effective molecular-assisted rates are attributed to differences in the production of H_2^+ and H^-. The Eirene simulations consider elastic scattering of H_2 and H with the background plasma, which is not evolved during the simulations. Neither of the Eirene setups include neutral-neutral interactions. As a result, the transport of molecules is independent of the atomic populations and vice versa. The electron temperatures are assumed sufficiently high and the molecular densities sufficiently low at divertor-relevant conditions to omit recombination of atoms and ions into molecules. Consequently, the molecular species are independent of the atomic populations. Subsequently, the recombination into atoms is omitted and the ionization rate of the atoms is artificially increased so that the atoms ionize upon creation. Consequently, computational resources are not spent on evaluating the atomic populations, which do not interact with the molecules analysed in this work.

The Eirene metastable-unresolved setup considers the H_2 depletion rates given in Table 1. The local molecular sinks are calculated using effective rates for the H_2 depletion processes as given in the AMJUEL database.[13] The CR model used to calculate the effective AMJUEL rates and the processes considered for each of the reaction types is explained below.

The CR model used to derive the AMJUEL rates, based on the CR model by Sawada and Fuijimoto,[14] was developed as an internal tool for producing A&M data for Eirene, but maintenance of the code has recently been discontinued. The CR model is capable of considering a large number of species, reactions, and transitions without making any assumptions regarding the plasma parameters. At Eirene's conceptualization, technical limitations necessitated the use

TABLE 1 Reactions included in the metastable-unresolved and metastable-resolved Eirene setups, respectively

Reaction name	Reaction	Metastable-unresolved	Metastable-resolved
Neutral dissociation (ND)	$e^- + H_2 \rightarrow e^- + 2H$	H.4 2.2.5g	H.2 2.vl1[a]
Ion conversion (IC)	$p^+ + H_2 \rightarrow H + H_2^+$	H.2 3.2.3	H.2 2.vl2[a]
Dissociative electron attachment (DEA)	$e^- + H_2 \rightarrow H + H^-$	H.2 2.2.17	H.2 2.vl3[a]
Electron impact ionization (EI)	$e^- + H_2 \rightarrow e^- + H_2^+ + e^-$	H.4 2.2.9	H.2 2.vl4[a]
Dissociative ionization (DI)	$e^- + H_2 \rightarrow e^- + H + H^+ + e^-$	H.4 2.2.10	H.4 2.2.10

Note: The reaction prefixes define whether electronic transitions are considered (H.4) or not (H.2) and "v" refers to the vibrational state. Both models consider elastic scattering with the plasma ions and the metastable-resolved model considers the ladder-like vibrational transitions given in H2VIBR.
[a] All reaction rate coefficients are taken from the AMJUEL database, except for those marked by "a", which are taken from the H2VIBR database.

of pre-computed fits and tabulated data, which necessitate a reduction in dimensionality to depend on one or two parameters, for communication between Eirene and the CR code. Consequently, ion-electron equilibration ($T_e = T_i$) and an effective charge of unity ($n_e = n_i$) are assumed in the AMJUEL database, which consists of reaction cross-sections and rate coefficient fits.

The available AMJUEL molecular reaction rate coefficients calculated by the CR model are divided into H.2, H.3, and H.4-type fits depending on the CR processes considered. The H.2 fits are dependent on the assumed common ion-electron temperature T only and do not consider electronic transitions or the target particle velocity in case of proton-impact reactions. The H.3 fits are used for heavy-particle reactions only, such as proton-impact reactions, and are functions of the reactant energy and plasma temperature, (V_{H_2}, T), where V_{H_2} is the individual H_2 velocity. The H.4 fits consider electronic transitions and are dependent on both electron density n_e and plasma temperature, (n_e, T). The n_e-dependence is due to the collisional electron excitation processes having an explicit dependence on the electron density, while the depopulating radiative decay is density-independent. The CR model considers transitions out of the electronic ground state of H_2 and multi-step electronic transitions resulting in the reaction products, but does not consider radiative decay back into the electronic ground state of H_2. Thus, any molecule that is electronically excited is eventually dissociated, resulting in an increased H_2 depletion rate. In AMJUEL, molecular reactions involving protons can either include electronic transitions, assuming the molecules to be at rest (H.4), omit electronic transitions and consider the energy of the molecules (H.3), or neither but not both. Herein the electron temperature and densities are used to represent the common electron-ion temperature and density assumed in the CR model. The CR models are zero-dimensional and do not explicitly consider transport of the condensed species. Thus, the resulting effective AMJUEL rates derived using the CR model assume local equilibrium, considering the reactions specified in the CR model.

The metastable-unresolved setup considers effective ion conversion (IC) and dissociative electron attachment (DEA) rates that do not include electronic transitions, as indicated by the H.2 prefix (Table 1). The IC rates assume the individual molecules to be at rest ($E_{H_2} = 0.1$ eV) and are, thus, independent of V_{H_2}. The CR model calculates the effective IC and DEA rates considering all possible collisional vibrational transitions, assuming H_2 to be at the local vibrational equilibrium distribution $P_{eq}(v)$. The neutral dissociation (ND), electron impact ionization (EI), and dissociative ionization (DI) rates are calculated by the CR model considering electronic transitions, as indicated by the H.4 prefix (Table 1). The EI and DI vibrational rates are derived assuming the molecules to be in their vibrational ground state, whereas the ND rates consider all possible collisional vibrational transitions, thus, assuming H_2 to be at $P_{eq}(v)$. As the different rates consider different processes impacting the vibrational distribution, or assume the molecules to be in their ground state, the implicit vibrational distribution of the sole molecular species in the metastable-unresolved setup will have an effective vibrational distribution different from the local equilibrium vibrational distribution $P_{eq}(v)$.

The metastable-resolved Eirene setup individually considers transport and evaluates the sinks for each of the 15 vibrational H_2 vibrational species, considering the depletion processes in Table 1. The vibrationally dependent ND, IC, DEA, and EI reaction rates used by the metastable-resolved Eirene setup are given in the H2VIBR database.[15] Each of the vibrationally resolved rates are taken as H.2 reaction rates of the molecular ground state without coupling to the electronically excited states. The vibrationally resolved reaction rates are derived by scaling the ground state rates as given in the HYDHEL database[16] according to the potential energy of the vibrational state as presented in ref.[17] The H2VIBR IC rates are derived assuming the individual molecules to be at rest ($E_{H_2} = 0.1$ eV). Vibrationally dependent DI rates are not

available in H2VIBR so the effective AMJUEL rates are used. The H2VIBR rates considers ladder-like vibrational transitions ($e^- + H_2(v) \rightarrow e^- + H_2\left(v' = v \pm 1\right)$) only. Thus, the metastable-resolved setup used does not consider H_2 depletion via electronically excited states or off-diagonal ($v \rightarrow v \pm N, N > 1$) vibrational transitions.

This work considers hydrogen plasmas as the AMJUEL and H2VIBR rates are given for hydrogen. The appropriate scalings of the hydrogen rates to account for isotopologue (D_2, T_2) effects have not yet been established: DEA has been shown to be dependent on the isotopologue[18] whereas the ND rate does not display an isotopologue effect.[19] Thus, the H_2 rates available in AMJUEL and H2VIBR cannot be directly scaled to account for isotopologue effects. Further work is required to establish the appropriate reactions and rates to be considered for heavier isotopologues and they have, thus, been omitted from this work.

2.2 | The Yacora collisional-radiative model

As the CR model used to derive the AMJUEL rates is no longer maintained, this work uses the continuously maintained and developed solver Yacora[20] to evaluate CR effects. Yacora is a flexible, modern solver for sets of coupled ordinary differential equations, such as CR systems, capable of evaluating non-linear and time-dependent processes. Yacora uses a comprehensive, up-to-date set of A&M data[21] and can also solve systems of equations using user-defined rate data. Here, Yacora is used to calculate the transport-free vibrational equilibrium distribution $P_{\mathrm{eq}}(v)$ using two sets of rates: (a) the "standard" Yacora A&M data (standard Yacora) as given in ref. [21] and (b) the metastable-resolved H_2 depletion rates in H2VIBR as listed in Table 1 (H2VIBR-Yacora). The standard Yacora data considers electronically excited states, including vibrationally resolved radiative decay into the molecular ground state resulting in vibrational re-distribution via electronically excited states, and off-diagonal vibrational transitions. The latter H2VIBR-Yacora setup only considers ladder-like vibrational transitions and uses user-supplied metastable-resolved rates. The rates are supplied to Yacora as tabulated data as a function of temperature and density, with 500 data points for the common ion-electron temperature distributed logarithmically in the interval $0.01\,\mathrm{eV} < T_e < 500\,\mathrm{eV}$ for plasma densities $n \in \left\{1 \times 10^{19}\ \mathrm{m}^{-3}, 1 \times 10^{20}\ \mathrm{m}^{-3}, 1 \times 10^{21}\ \mathrm{m}^{-3}\right\}$.

3 | RESULTS

3.1 | Verification of Eirene transport-free simulations using Yacora

To compare the Eirene metastable-resolved $P_{\mathrm{eq}}(v)$ predictions against Yacora, the reaction rates need to be common between the codes. This is realized using the H2VIBR-Yacora model with user-supplied metastable-resolved rates. As Yacora performs zero-dimensional calculations, transport effects must be omitted from the Eirene simulations. This was achieved by evaluating a Cartesian cell with reflective boundaries and prescribed, common ion-electron temperature and density. The temperature was varied to retain parameter scans in temperature for the densities $n \in \left\{1 \times 10^{19}\ \mathrm{m}^{-3}, 1 \times 10^{20}\ \mathrm{m}^{-3}, 1 \times 10^{21}\ \mathrm{m}^{-3}\right\}$. The cell is supplied by a central 1A source of electronic and vibrational ground state molecules and the Eirene simulations were performed using 5×10^5 histories and 160 s CPU runtime.

The Eirene and Yacora predictions are within 10% with largest discrepancy for $T_e = 10$ eV (Figure 1). As T_e decreases towards 1 eV, the impact of molecular processes is expected to be negligible since the volumetric recombination rate increases strongly, resulting in recombination-dominated plasmas where atomic processes dominate. For temperatures in excess of 5 eV, the dissociation and ionization rates increase strongly, resulting in low H and H_2 densities and an ionization-dominated plasma. Thus, this work focuses on the temperature range in the interval 1–5 eV, where molecular effects are expected to be significant. For temperatures in excess to 5 eV, the H_2 depletion rates are high, and increase with the vibrational quantum number v, resulting in weakly populated $v \gtrsim 4$ vibrational states and poor statistics, explaining the discrepancy between the codes at $T_e = 10$ eV. The vibrational distributions show a negligible dependence on density as only the DI rates are dependent on density and the density dependence of the DI rates have a negligible impact on the equilibrium vibrational distribution.

The agreement between the metastable-resolved and metastable-unresolved setup cannot be assessed by comparing the vibrational distributions of the setups since the H_2 vibrational distribution is not explicitly available from the metastable-unresolved Eirene simulations. Instead, the agreement is assessed by comparing the effective dissociation rates predicted by the simulations. The effective dissociation rate ($\langle \sigma v \rangle_{\mathrm{diss}}^{\mathrm{eff}}(T_e, n_e)$) can be solved from the effective

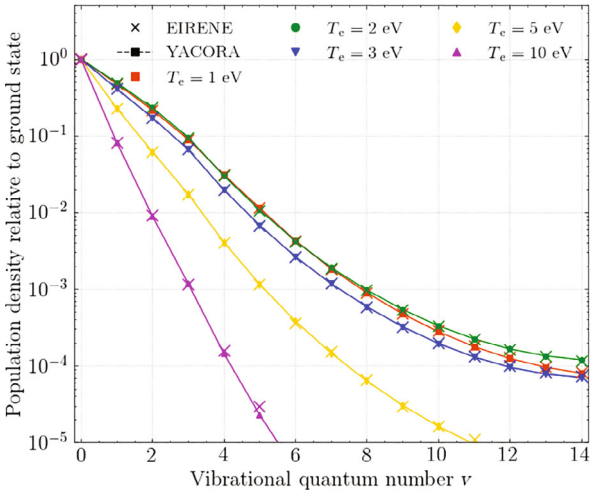

FIGURE 1 Vibrational population of H_2 relative to the H_2 ground state for plasma density $n = 1 \times 10^{20}$ m^{-3} predicted by the metastable-resolved Eirene setup (×) and the H2VIBR-Yacora model (−)

dissociation sink $S^{\text{eff}}_{\text{diss}}$ calculated by the metastable-unresolved Eirene simulations:

$$\frac{S^{\text{eff}}_{\text{diss}}}{V} = \sum_r n_e n_{\text{H}_2} \langle \sigma v \rangle^r_{\text{diss}} (T_e, n_e) = n_e n_{\text{H}_2} \langle \sigma v \rangle^{\text{eff}}_{\text{diss}} (T_e, n_e) \rightarrow \langle \sigma v \rangle^{\text{eff}}_{\text{diss}} (T_e, n_e) = \frac{S^{\text{eff}}_{\text{diss}}}{V n_e n_{\text{H}_2}}. \tag{1}$$

Here $S^{\text{eff}}_{\text{diss}}$ is the effective dissociation sink in s^{-1}, V the domain volume, n_e and n_{H_2} refer to the electron and H_2 densities, respectively, and $\langle \sigma v \rangle^r_{\text{diss}} (T_e, n_e)$ is the reaction rate coefficient for the H_2 depletion process r.

For the metastable-resolved simulations, the dissociation sink is calculated for each vibrational state v, necessitating a generalization of Equation (1):

$$\begin{aligned} \frac{S^v_{\text{diss}}}{V} &= \sum_r n_e n_{\text{H}_2(v)} \langle \sigma v \rangle^{v,r}_{\text{diss}} (T_e, n_e) \\ \rightarrow \langle \sigma v \rangle^{\text{eff}}_{\text{diss}} (T_e, n_e) &= \frac{\sum_v n_{\text{H}_2(v)} \langle \sigma v \rangle^{v,\text{eff}}_{\text{diss}} (T_e, n_e)}{\sum_v n_{\text{H}_2(v)}} = \frac{\sum_v S^v_{\text{diss}}}{V n_e \sum_v n_{\text{H}_2(v)}}, \end{aligned} \tag{2}$$

where S^v_{diss} and $\langle \sigma v \rangle^{v,r}_{\text{diss}} (T_e, n_e)$ are the dissociation sink in s^{-1} and the reaction rate coefficient for the H_2 depletion process r, respectively, for vibrational state v.

The metastable-resolved Eirene setup systematically yields dissociation rates 25% lower than the metastable-unresolved Eirene setup, which increases to 65% for $T_e = 1$ eV for plasma density $n = 1 \times 10^{20}$ m^{-3} (Figure 2). By progressively matching the rates between the metastable-resolved and metastable-unresolved setups, the impact of the different rates can be resolved.

Using AMJUEL rate H.4 2.2.9 as the EI rate in the metastable-resolved setup improves the agreement between the setups for all $T_e > 2$ eV, removing most of the systematic difference for $T_e > 8$ eV (Figure 2, red line). AMJUEL rate H.4 2.2.9 assumes the molecules to be in their ground vibrational state and considers electronic transitions, indicating the role of vibrational excitation and electronic transitions on the EI channel to be significant for plasma temperatures in excess of 6 eV. Using the H_2 vibrational ground state ND rate H2VIBR H.2 2.0l1 for all molecular species in both setups further improves the agreement for $T_e > 1.5$ eV (Figure 2, blue line). Thus, multi-step ND via electronically excited states and off-diagonal vibrational transitions $v \rightarrow v \pm N, N > 1$, considered by AMJUEL rate H.4 2.2.5g but not by H2VIBR rate H.2 2.0l1, are significant in the plasma temperature interval 1.5 eV $< T_e <$ 10 eV. Using AMJUEL rate H.2 3.2.3 for IC in the metastable-resolved setup further improves the agreement between the setups for $T_e < 4$ eV (Figure 2, cyan line), indicating that the off-diagonal vibrational transitions are significant for the IC reaction when $T_e < 4$ eV. The remaining difference between the metastable-resolved and unresolved effective dissociation rates for $T_e < 1.5$ eV (Figure 2, cyan line)

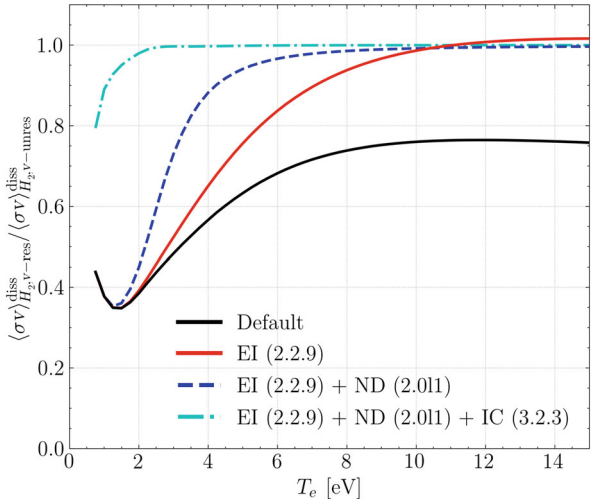

FIGURE 2 Ratio of the effective dissociation rates for the metastable-resolved Eirene setup to that of the metastable-unresolved Eirene setup as a function of plasma temperature shown for plasma density $n = 1 \times 10^{20}$ m^{-3}. The different lines show the effects of progressively matching the different rates, for example, for the red line both the metastable-resolved and metastable-unresolved Eirene simulations use AMJUEL rate 2.2.9 for electron impact ionization, and for the cyan line only the dissociative electron attachment rates differ between the setups

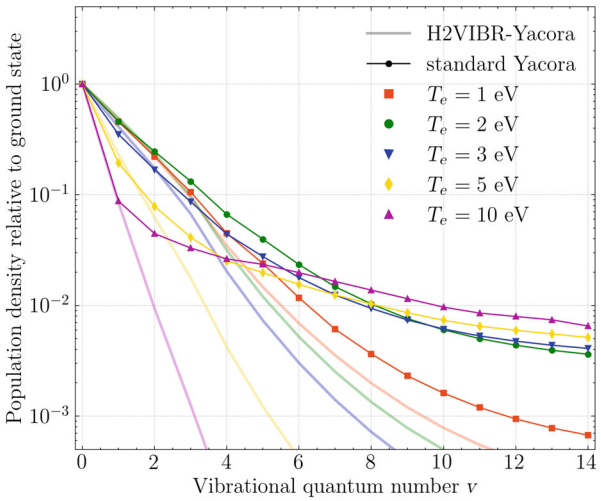

FIGURE 3 Vibrational population densities relative to the ground state for plasma density $n = 1 \times 10^{20}$ m^{-3} predicted by the standard Yacora model superimposed on the corresponding H2VIBR-Yacora predictions

is due to differences in the DEA rates used by the setups. The metastable-unresolved setup uses AMJUEL rate H.2 2.2.17 for DEA that considers off-diagonal vibrational transitions that the metastable-resolved H2VIBR rates do not consider, which affect the DEA rates when $T_e < 1.5$ eV.

The effective rates were evaluated in the temperature range $T_e = 0.75 - 15$ eV, which includes the interval 1 eV $< T_e < 5$ eV where the impact of molecular effects is assumed to be the largest. For higher temperatures, the plasmas are ionization-dominated, and the molecular densities are expected to be negligible. For $T_e < 1$ eV, the plasmas are recombination-dominated, and atomic effects are dominant. In addition, the rate coefficient fits are only applicable for $T_e > 0.5$ eV and all rates decrease exponentially for $T_e < 1$ eV, resulting in long computational times and zero-divisors when comparing the rates for $T_e < 0.75$ eV.

Standard Yacora simulations, using the full set of Yacora A&M data, predicts a H_2 vibrational distribution shifted to higher vibrational quantum number compared to the H2VIBR-Yacora simulations (Figure 3). This shift

is caused by different reaction rates used by the codes and inclusion of additional CR processes in Yacora compared to the metastable-resolved Eirene setup. These processes include H_2 depletion via excited electronic states, off-diagonal vibrational transitions, and vibrational re-distribution via electronically excited states. The role of vibrational re-distribution via electronic states is negligible for $T_e \leq 5$ eV, but likely contributes to the shift of the vibrational distribution to higher vibrational quantum number observed for $T_e \geq 5$ eV[22,23] (Figure 3). As the reaction rates of most H_2 depletion processes increase strongly with the vibrational quantum number, the observed shift of the vibrational distribution compared to the metastable-resolved vibrational distribution may explain the observed decrease in effective dissociation rate of the metastable-resolved Eirene setup compared to the metastable-unresolved setup. However, further work is required to assess the impact of each of the aforementioned processes on the effective reaction rate.

The metastable-resolved Eirene setup cannot capture two potentially significant CR effects that are considered by the AMJUEL effective rates used in the metastable-unresolved setup: H_2 depletion via electronic excitation and off-diagonal vibrational transitions. Neither the metastable-resolved nor metastable-unresolved Eirene setups consider vibrational re-distribution via electronically excited states: however, the effect of this process is expected to be negligible under conditions when molecular processes are expected to be relevant, $T_e < 5$ eV. The decrease in effective dissociation rate for the metastable-resolved setup compared to the metastable-unresolved setup is attributed to the omitted CR processes, which affects the local vibrational equilibrium and, subsequently, the effective dissociation rate.

3.2 | The role of non-local transport phenomenon

Transport of vibrationally excited states may result in non-local effects, which are not considered by CR models. If the vibrational equilibration mean-free path ($\lambda_{mfp}^{P_{eq}}$) exceeds the spatial discretization of the numerical domain, the metastable, vibrational species are transported out of the cell that is analysed before achieving $P_{eq}(v)$. Subsequently, the vibrational molecular distribution will be shifted towards the distribution of the molecular source, such as the initial vibrational state of the molecules that are recycled at the wall.

Metastable-resolved Eirene simulations are performed for a simplified, Cartesian geometry that does not consider recycling at the boundaries to approximate $\lambda_{mfp}^{P_{eq}}$. The numerical domain consists of a single cell with dimensions $L \times L$ and a third dimension that is defined so that its volume is maintained constant independent of L. The cell is surrounded by eight "guard" cells to capture the effects of molecular back-scattering from the neighbouring cells. Any fluxes that reach the domain boundary beyond the cells are removed. The central cell is prescribed a central 1 A vibrational ground state molecular source. The domain is assigned a constant plasma temperature and density: the temperature is varied in the interval $0.5\ \text{eV} < T_e < 15\ \text{eV}$ for $n \in \left\{1 \times 10^{19}\ \text{m}^{-3}, 1 \times 10^{20}\ \text{m}^{-3}, 1 \times 10^{21}\ \text{m}^{-3}\right\}$. Parameter scans are performed for side lengths $L \in \{0.5\ \text{cm}, 1\ \text{cm}, 5\ \text{cm}, 20\ \text{cm}\}$ and compared to the equilibrium vibrational distribution $P_{eq}(v)$ to obtain an approximation for $\lambda_{mfp}^{P_{eq}}$. When $P_{eq}(v)$ is obtained by the metastable-resolved Eirene simulations, half the cell side length $L/2$ is considered to be in excess of $\lambda_{mfp}^{P_{eq}}$. Here, the fraction of molecules in their ground vibrational state is taken to be representative of $P_{eq}(v)$.

The vibrational equilibration mean-free path is found to be $\gg 10$ cm, ~ 10 cm, and ~ 2.5 cm for plasma background densities of $1 \times 10^{19}\ \text{m}^{-3}$, $1 \times 10^{20}\ \text{m}^{-3}$, and $1 \times 10^{21}\ \text{m}^{-3}$, respectively (Figure 4). Fine grids are necessary close to the target to resolve the temperature and density gradients and to reduce the discretization error. Thus, plasmas with densities below $n = 1 \times 10^{21}\ \text{m}^{-3}$ are not expected to be vibrationally equilibrated close to the divertor targets. As plasma densities, even under detachment, typically are not expected to significantly exceed $n = 1 \times 10^{21}\ \text{m}^{-3}$, transport of vibrational states is expected to impact the vibrational distribution and the effective molecular dissociation sink.

Eirene simulations of pure hydrogen plasmas are performed on a 300 cm × 1 cm one-dimensional flux-tube to assess the impact of non-local transport effects. The 112 × 1 cell plasma grid and background plasmas are generated by the multi-fluid plasma code UEDGE[24] for ion and electron upstream volumetric power sources of 4 and 9 kW, respectively. The ion-electron power distribution is determined by matching the upstream temperature ratios of two-dimensional, sheath-limited plasma simulations. A variable upstream particle source supplies the plasma particles, and the resulting upstream density is taken as the independent parameter. The target temperature and density predictions are presented in Figure 5. The simulations were performed for $B_{tot} = 5$ T and $B_\theta = 0.3$ T with reflecting radial and upstream boundary conditions. The Eirene simulations assume 1% pumping of atoms and molecules at the target and the remaining target fluxes are recycled as vibrational ground-state molecules to match the target molecular source between the metastable-resolved

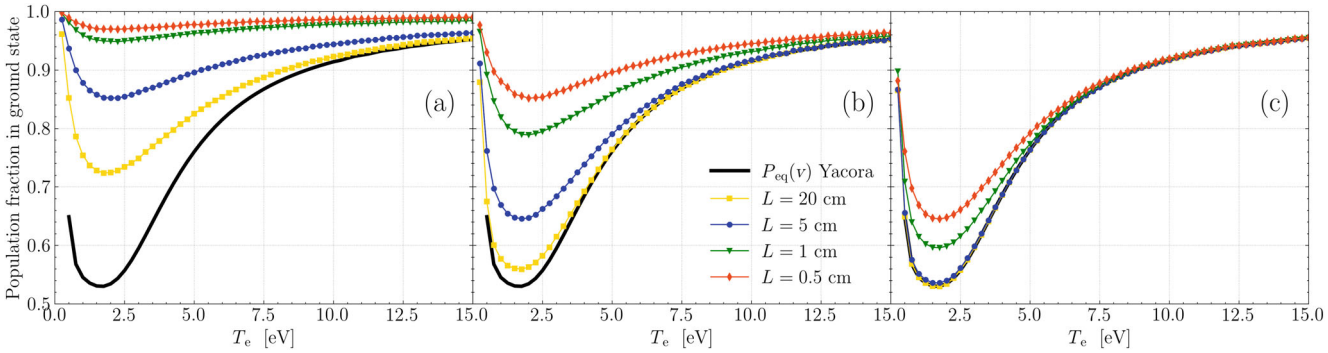

FIGURE 4 Population fraction in the vibrational H_2 ground state as a function of temperature for plasma density $n = 1 \times 10^{19}$ m^{-3} (a), $n = 1 \times 10^{20}$ m^{-3} (b), and $n = 1 \times 10^{21}$ m^{-3} (c) for varying cell side-length L. The vibrational equilibrium distribution $P_{eq}(v)$ is calculated by the H2VIBR-Yacora setup, assuming local vibrational equilibrium

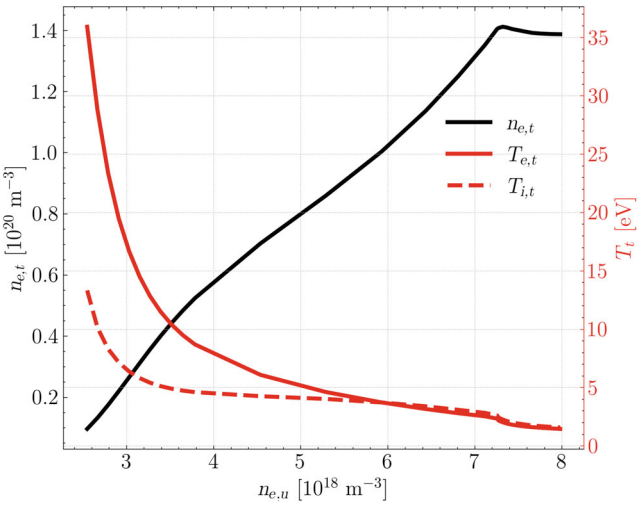

FIGURE 5 Target plasma density (left ordinate) and ion (- -) and electron (–) temperature (right ordinate) profiles as a function of the upstream density predicted by the multi-fluid code UEDGE and used as background plasmas for the Eirene simulations

and metastable-unresolved Eirene setups. To compare the metastable-resolved and metastable-unresolved Eirene setups without feedback between the neutral and plasma predictions, the Eirene simulations are not coupled to the fluid plasma simulations.

The metastable-unresolved Eirene predictions show that the molecules do not reach $P_{eq}(v)$ along the flux tube before being transported upstream and dissociated for the $n_{e,u} = 8.0 \times 10^{18}$ m^{-3} simulation (Figure 6). The target fluxes are recycled as ground-state H_2, which travel upstream before being vibrationally excited. As the vibrational equilibration mean-free path is ~2.5 cm, the vibrational distribution within ~1 cm of the target is shifted towards the initial vibration distribution, which is ground-state H_2 only. Between 1 and 2 cm from the target, the Eirene-predicted vibrational distribution is shifted to higher vibrational state than $P_{eq}(v)$ due to non-local transport effects. The corresponding H_2 densities are reduced by 50 and 85% compared to the target, respectively, due to increasing temperature and dissociation source strength. The temperature gradients result in molecular density two orders of magnitude lower than at the target 5 cm upstream of the target. As a result of the exponentially decreasing molecular densities, the dissociation strength is leveraged towards the target vibrational population distribution, which is shifted to lower vibrational state compared to $P_{eq}(v)$, resulting in a smaller dissociation sink. For decreasing $n_{e,u}$, the target temperature increases, resulting in increasing molecular dissociation and lower molecular densities, especially for $n_{e,u} < 5.4 \times 10^{18}$ m^{-3} as $T_{e,t} > 5$ eV (Figure 5). Thus, it is expected that the significance of transport effects decreases with $n_{e,u}$ and differences in the molecular dissociation rates and densities for $n_{e,u} \lesssim 5.4 \times 10^{18}$ m^{-3} are due to differences in the H_2 depletion rates between the metastable-resolved and metastable-unresolved Eirene model.

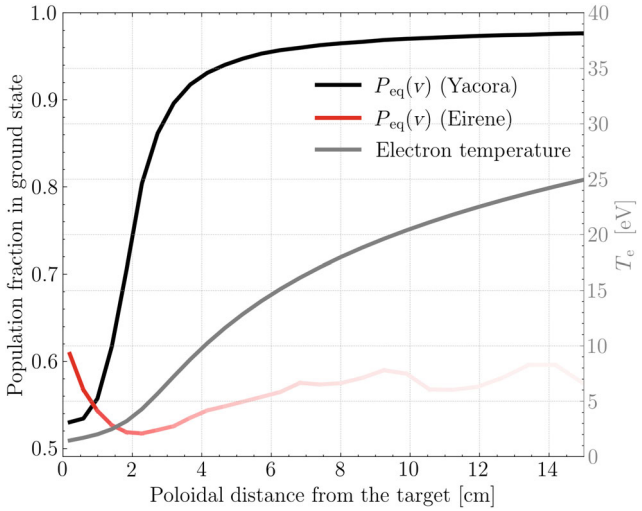

FIGURE 6 Poloidal profile of the population fraction in the vibrational H_2 ground state (left ordinate) predicted by the metastable-resolved Eirene setup (red) and $P_{eq}(v)$ as predicted by H2VIBR-Yacora (black) for $n_{e,u} = 8.0 \times 10^{18}$ m^{-3}. Also shown is the electron temperature (grey, right ordinate). The opacity of the Eirene-predicted vibrational distribution corresponds to the logarithmic ratio of H_2 density to the target H_2 density

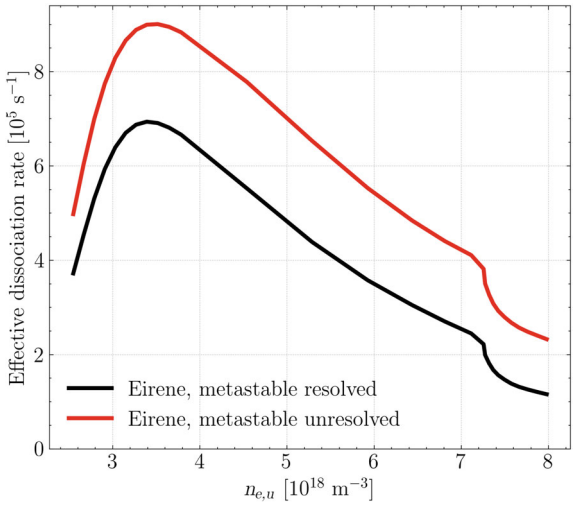

FIGURE 7 Effective dissociation sink for the metastable-unresolved (red) and metastable-resolved (black) Eirene setups as a function of upstream electron density. The effective dissociation sink is taken as the integrated dissociation sink in the flux tube normalized to the molecular content

The metastable-resolved Eirene model predicts a 30% decrease in the effective dissociation rate under sheath-limited conditions, which increases to 50% under detached conditions, compared to the metastable-unresolved setup (Figure 7). Here, the effective dissociation sink is taken to be $S_{\text{diss}}^{\text{eff}} = \int (S_{\text{diss}}/V) dV / \int n_{H_2} dV$, where the dissociation rate S_{diss} is the Eirene-predicted dissociation sink in s^{-1} and the integration is performed over the whole flux-tube. Under sheath-limited conditions, the role of transport of metastable states is expected to be small due to target temperatures in excess of 5 eV strongly dissociating all molecules regardless of their vibrational state (Figure 5). Thus, the observed 30% decrease in the effective dissociation sink for the metastable-resolved setup compared to the metastable-unresolved setup is mainly due to omission of relevant CR processes, which resulted in a decreased effective dissociation rate in transport-free Eirene simulations (Figure 2). Under detached conditions, molecular densities and processes are significant and transport of vibrational states is expected to become relevant. This is observed as 50% lower effective dissociation rates for the metastable-resolved setup compared to the metastable-unresolved setup predicted by Eirene for $n_{e,u} > 7 \times 10^{18}$ m^{-3}. This result is indicative of the role of transport of vibrational states being significant at the detachment onset, while being

negligible under sheath- and conduction-limited conditions. However, the metastable-resolved reaction rates do not consider all CR processes included in the metastable-unresolved rates. Thus, the decrease in effective dissociation rate for the metastable-unresolved model compared to the metastable-resolved model includes the net effect of both transport of metastable, vibrational states, and the impact of CR processes. Subsequently, the impact of non-local transport effects cannot be independently assessed using the reaction rates presently available in AMJUEL and H2VIBR.

4 | CONCLUSIONS

A 30–50% decrease in the effective dissociation rate is observed in one-dimensional flux-tube simulations of pure hydrogen plasmas using a metastable-resolved Eirene setup, compared to when a metastable-unresolved setup was used. The decrease is found to be caused by two mechanisms: (a) the available metastable-resolved H2VIBR rates do not consider off-diagonal vibrational transitions $v \rightarrow v \pm N, N > 1$ or depletion of hydrogen molecules due to electron excitation and (b) non-local effects caused by transport of metastable vibrationally excited states. The difference in rates for the metastable-resolved Eirene model is found to cause up to 65% decrease in the effective dissociation rates, dependent on the local plasma temperature, compared to the metastable-unresolved setup in transport-free simulations. Thus, the simulations of the one-dimensional flux-tube includes the contribution of the differences between the metastable-resolved and metastable-unresolved Eirene setups caused by CR processes and non-local transport effects. When accounting for the differences in the reaction rates due to CR processes between the setups, non-local effects caused by transport are expected to be relevant under detached conditions only. The metastable-resolved reaction rates available to the Eirene simulations omit the aforementioned CR processes. As the two effects cannot presently be evaluated separately in Eirene, it is not possible to conclusively determine to what degree transport of metastable, vibrationally excited states will impact SOL plasma simulations.

The decreased dissociation rate predicted by the metastable-resolved Eirene setup compared to the metastable-unresolved Eirene setup will result in fewer atomic and molecular particles. Consequently, the momentum exhaust by plasma-neutral friction and radiative losses are reduced, as atoms are a more efficient radiator than molecules at divertor-relevant conditions. Both effects are expected to decrease the degree of detachment, all other things equal, supporting the findings of ref. [11]. However, the net effect when accounting for plasma-neutral interaction has not been considered in this work and coupled plasma-neutral simulations should be performed to evaluate the role of this plasma-neutral interaction.

The present metastable-resolved model could be extended by adding (n_e, T)-resolved rates that include excited electronic states, or (V_{H_2}, T)-dependent rates, which take the molecular energy into account, to the H2VIBR database. However, the CR model used to produce the AMJUEL and H2VIBR rates has been phased out and is no longer available to the community. To update the A&M data used by Eirene, the CR code, which represents the understanding of A&M data and CR processes from the early 2000s, must be recommissioned and updated. In addition, the communication between Eirene and the CR code via tabulated data or fits restricts the dimensions that can be resolved to two. Thus, the impact of electronically excited states, resulting in a density-dependence, cannot be evaluated simultaneously as the impact of V_{H_2} dependent rates or thermally unequilibrated ions and electrons.

Ideally, real-time communication between Eirene and a CR model, such as Yacora, should be implemented to enable simultaneous evaluation of all relevant CR effects and transport. Such a coupling would allow for evaluation of thermally unequilibrated plasmas, simultaneous evaluation of electronically excited states and their V_{H_2}-dependence, and off-diagonal vibrational transitions. Real-time communication between Eirene and a CR code would enable consideration of processes that may be significant, such as vibrational re-distribution via electronically excited states and inclusion of first-order data of electronic and vibrational transitions. In addition, true isotopologue effects could be considered by including reaction rates for different isotopologues where available, rather than internally re-scaling the hydrogen reaction rates as is presently done for simulations of isotopologues in Eirene.

ACKNOWLEDGEMENTS

The authors would like to thank Professor U. Fantz and Professor D. Reiter for valuable discussions enabling this work. This work has been carried out within the framework of the EUROfusion Consortium and has received funding from the Euratom research and training programme 2014–2018 and 2019–2020 under grant agreement number 633053. The views and opinions expressed herein do not necessarily reflect those of the European Commission. This work was supported by the Academy of Finland under grant no. 13330050.

CONFLICT OF INTEREST

The authors declare no potential conflict of interests.

AUTHOR CONTRIBUTIONS

Andreas Holm was responsible for the conceptualization, investigation, and writing—original draft. Mathias Groth was responsible for coordination and project management. Dirk Wünderlich was responsible for the Yacora simulations. Petra Börner assisted with and validated the Eirene simulation setup.

DATA AVAILABILITY STATEMENT

The data that support the findings of this study are available upon request from the author. The data is stored in the directory m/phys/project/fusion/holma2/2021/pet on the Triton cluster of Aalto University.

REFERENCES

[1] D. Reiter, M. Baelmans, P. Börner, *Fusion Sci. Technol.* **2005**, *47*(2), 172.
[2] S. Wiesen, D. Reiter, V. Kotov, M. Baelmans, W. Dekeyser, A. Kukushkin, S. Lisgo, R. Pitts, V. Rozhansky, G. Saibene, G. Saibene, I. Veselova, S. Voskoboynikov, *J. Nucl. Mater.* **2015**, *463*, 480.
[3] X. Bonnin, W. Dekeyser, R. Pitts, D. Coster, S. Voskoboynikov, S. Wiesen, *Plasma and Fusion Res.* **2016**, *11*, 1403102.
[4] Y. Feng, F. Sardei, J. Kisslinger, P. Grigull, K. McCormick, D. Reiter, *Contrib. Plasma Physics* **2004**, *44*(1–3), 57.
[5] R. Simonini, G. Corrigan, G. Radford, J. Spence, A. Taroni, *Contrib. Plasma Physics* **1994**, *34*(2–3), 368.
[6] S. Wiesen, Edge2d/eirene code interface report, 2006, http://www.eirene.de/e2deir_report_30jun06.pdf, (accessed: September 23, 2021).
[7] S. Brezinsek, P. Greenland, P. Mertens, A. Pospieszczyk, D. Reiter, U. Samm, B. Schweer, G. Sergienko, *J. Nucl. Mater.* **2003**, *313–316*, 967.
[8] S. Markelj, I. Čadež, *J. Chem. Phys.* **2011**, *134*, 124707.
[9] H. P. Summers, M. G. O'Mullane, AIP Conference Proceedings, Vol. *1344*, American Institute of Physics, Vilnius, Lithuania **2011**, p. 179.
[10] U. Fantz, B. Heger, D. Wünderlich, *Plasma Phys. Control. Fusion* **2001**, *43*(7), 907.
[11] U. Fantz, D. Reiter, B. Heger, D. Coster, *J. Nucl. Mater.* **2001**, *290*, 367.
[12] K. Miyamoto, Y. Ishii, A. Hatayama, *J. Appl. Phys.* **2003**, *93*(2), 845.
[13] D. Reiter, The data file amjuel: Additional atomic and molecular data for eirene, **2020**, http://eirene.de/amjuel.pdf (accessed: September 2021).
[14] T. Fujimoto, K. Sawada, *J. Appl. Phys.* **1995**, *78*, 2913.
[15] D. Reiter, The data file H2VIBR: Additional Molecular Data for EIRENE: vibrationally resolved $H_2(x)$ ground state, http://eirene.de/h2vibr.pdf (accessed: September 2021).
[16] D. Reiter, The data file HYDHEL: Atomic and Molecular Data for EIRENE based upon: Janev, Langer, Evans, Post. Elementary Processes in Hydrogen-Helium Plasmas, Springer 1987, http://eirene.de/hydhel.pdf (accessed: September 2021).
[17] P. T. Greenland, D. Reiter, The role of molecular hydrogen in plasma recombination, Forschungszentrum Jülich, Zentralbibliothek, Jülich **1996**.
[18] J. Bardsley, J. Wadehra, *Phys. Rev. A* **1979**, *20*, 1398.
[19] L. H. Scarlett, D. V. Fursa, J. Knol, M. C. Zammit, I. Bray, *Phys. Rev. A* **2021**, *103*, L020801.
[20] D. Wünderlich, S. Dietrich, U. Fantz, *J. Quant. Spectrosc. Radiat. Transf.* **2009**, *110*(1–2), 62.
[21] D. Wünderlich, U. Fantz, *Atoms* **2016**, *4*(4), 26.
[22] R. Celiberto, M. Capitelli, U. Lamanna, *Chem. Phys.* **1994**, *183*(1), 101.
[23] J. Hiskes, *J. Appl. Phys.* **1980**, *51*, 4592.
[24] T. Rognlien, M. Rensink, G. Smith, Users manual for the UEDGE edge-plasma transport code, **2000**, https://github.com/LLNL/UEDGE (accessed: September 2021).

How to cite this article: A. Holm, D. Wünderlich, M. Groth, P. Börner, *Contributions to Plasma Physics* **2022**, *62*(5-6), e202100189. https://doi.org/10.1002/ctpp.202100189